

# Multidimensional, high precision beam spin asymmetry measurements of semi-inclusive pion production off the proton with CLAS12

S. Diehl<sup>1,2\*</sup> for the CLAS collaboration

<sup>1</sup> II. Physikalisches Institut der Universität Gießen, 35392 Gießen, Germany

<sup>2</sup> University of Connecticut, Storrs, Connecticut 06269, USA

\* stefan.diehl@exp2.physik.uni-giessen.de

June 2, 2021

## 1 Abstract

High precision measurements of the polarized electron beam-spin asymmetry in SIDIS from the proton have been performed using a 10.6 GeV incident electron beam and the CLAS12 spectrometer at Jefferson Lab. The proceeding reports a multidimensional study of the structure function ratio  $F_{LU}^{sin\phi}/F_{UU}$  extracted from single pion ( $\pi^+$ ,  $\pi^-$ ,  $\pi^0$ ) SIDIS data over a large kinematic range in  $z$ ,  $x_B$ ,  $P_T$  and virtualities  $Q^2$  ranging from 1 GeV<sup>2</sup> up to 7 GeV<sup>2</sup>.  $F_{LU}^{sin\phi}$  is a twist-3 quantity that can reveal novel properties of quark-gluon correlations within the nucleon.

## 10 1 Introduction

Many decades of experiments in deep inelastic scattering (DIS) of lepton beams off nucleons have mapped out the momentum distributions of the partons in the nucleon in terms of one-dimensional parton distribution functions (PDFs) [1, 2]. While these measurements provided significant insight into the structure of the nucleon, many important and interesting aspects of the nucleon structure cannot be revealed in this one dimensional picture since PDFs are essentially averaged over all degrees of freedom except the longitudinal momentum. Therefore, they cannot address questions such as: Do quarks undergo orbital motion? Is there a connection between the motion of quarks, their spin and the spin of the proton? How is the total spin of the proton built up from the spin and the orbital angular momentum of partons? Today, the possibility of three-dimensional (3-D) imaging exists, which allows such questions to be addressed [3–5]. Remarkable theoretical advances over the past decade have led to a rigorous framework where information on the confined motion of the partons inside a fast moving nucleon is matched to transverse momentum dependent parton distribution functions (TMDs) [4, 6]. In particular, TMDs can encode information about the orbital motion of quarks in the parent nucleon and correlations between the motion of partons and their spin. Semi-inclusive DIS (SIDIS), where a specified hadron is detected in the final state, is a powerful tool to study the transverse momentum dependent partonic structure of the nucleon. Spin asymmetries in polarized SIDIS can be related to TMDs and fragmentation functions (FFs). Since beam single spin asymmetries (SSAs) are subleading twist-3 objects, they are expected to be suppressed by  $\mathcal{O}(M/Q)$ , where  $M$  is the target mass and  $Q^2$  is the photon virtuality. However, with the energies available at existing fixed-target facilities, contributions of the order  $\mathcal{O}(M/Q)$  could be sizable, making such twist-3 contributions accessible and thereby providing access to the information they contain about quark-gluon correlations.

35 The diagram in Fig.1(a) shows the SIDIS scattering process, including the involved  
 TMDs and FFs, and Fig. 1(b) shows the definition of the reaction kinematics.

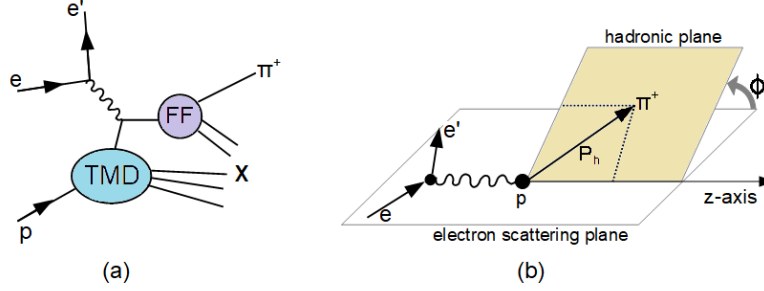


Figure 1: (a) Schematic diagram of the single pion semi-inclusive deep inelastic scattering process with the involved parton distributions and fragmentation functions. (b) Definition of the reaction kinematics of single pion SIDIS.

36

37 Beam SSAs are defined as:

$$SSA(z, P_T, \phi, x_B, Q^2) = \frac{d\sigma^+ - d\sigma^-}{d\sigma^+ + d\sigma^-} = \frac{A_{LU}^{\sin\phi} \sin\phi}{1 + A_{UU}^{\cos\phi} \cos\phi + A_{UU}^{\cos 2\phi} \cos 2\phi}, \quad (1)$$

38 where  $d\sigma^\pm$  is the differential cross section for the two beam helicity states ( $\pm$ ). The  
 39 subscripts of the moments  $A_{ij}$  represent the longitudinally polarized (L) or unpolarized  
 40 (U) state of the beam and the target. As defined in Fig.1 (b),  $\phi$  is the azimuthal angle  
 41 between the electron scattering and the hadronic reaction plane.

42 The  $\sin\phi$  moment  $A_{LU}^{\sin\phi}$  is directly related to the polarized structure function  $F_{LU}^{\sin\phi}$ :

$$A_{LU}^{\sin\phi} = \frac{\sqrt{2\epsilon(1-\epsilon)} F_{LU}^{\sin\phi}}{F_{UU,T} + \epsilon F_{UU,L}} = \sqrt{2\epsilon(1-\epsilon)} \frac{F_{LU}^{\sin\phi}}{F_{UU}}, \quad (2)$$

43 where  $F_{UU,T}$  and  $F_{UU,L}$  represent the contributions from transversely and longitudinally  
 44 polarized virtual photon, and  $\epsilon$  is the ratio of their fluxes.

45 The structure function  $F_{LU}^{\sin\phi}$ , which is related to the quark-gluon-quark correlations  
 46 in the proton can be expressed as a convolution ( $\mathcal{C}$ ), of TMDs and FFs [4, 7]:

$$F_{LU}^{\sin\phi} = \frac{2M}{Q} \mathcal{C} \left[ -\frac{\hat{\mathbf{h}} \cdot \mathbf{k}_T}{M_h} \left( x_B e H_1^\perp + \frac{M_h}{M} f_1 \frac{\tilde{G}^\perp}{z} \right) + \frac{\hat{\mathbf{h}} \cdot \mathbf{p}_T}{M} \left( x_B g^\perp D_1 + \frac{M_h}{M} h_1^\perp \frac{\tilde{E}}{z} \right) \right], \quad (3)$$

47 where  $e$  is a twist-3 PDF,  $H_1^\perp$  is the Collins FF,  $f_1$  is an unpolarized distribution function,  
 48  $\tilde{G}^\perp$  is a twist-3 FF,  $g^\perp$  is a twist-3 T-odd distribution function,  $D_1$  is an unpolarized FF,  
 49  $h_1^\perp$  is the Boer-Mulders function and  $\tilde{E}$  is a twist-3 FF [4, 8]. Furthermore,  $M_h$  is the pion  
 50 mass and  $\hat{\mathbf{h}}$  is a unit vector in the direction of the pions transverse momentum,  $\mathbf{p}_T$  and  
 51  $\mathbf{k}_T$  are the intrinsic quark transverse momentum in the generic distribution functions  $f_1$   
 52 and in the fragmentation function  $D_1$  [4].

## 53 2 Experimental procedures

54 In this work, we extract the structure function ratio  $F_{LU}^{\sin\phi}/F_{UU}$  in single pion SIDIS  
 55 of longitudinally polarized electrons off unpolarized protons with a wide range of fully  
 56 differential kinematics in the  $Q^2$  range from 1.7 to 7.0 GeV<sup>2</sup>,  $x_B$  from 0.13 - 0.52,  $z$  from

57 0.18 - 0.7 and  $P_T$  up to 0.85 GeV. Here we define the virtuality of the collision as  $Q^2$ , the  
 58 fraction of the proton's momentum carried by the struck quark as  $x_B$ , the energy fraction  
 59 of the virtual photon carried by the outgoing hadron as  $z$  and the transverse momentum  
 60 of the final state hadron as  $P_T$ .

61 The measurements were performed at Jefferson Lab with CLAS12 (CEBAF Large  
 62 Acceptance Spectrometer for experiments at 12 GeV) [9]. The incident electron beam  
 63 was longitudinally polarized and had an energy of 10.6 GeV. The target was unpolarized  
 64 liquid hydrogen. The CLAS12 forward detector consists of six identical sectors within a  
 65 toroidal magnetic field. The momentum and the charge of the particles were determined  
 66 by 3 regions of drift chambers. The electron identification was based on a lead-scintillator  
 67 electromagnetic sampling calorimeter in combination with a Cherenkov counter, while  
 68 positive pions were identified by time-of-flight measurements.

69 Deeply inelastic scattered electrons, were selected by cuts on  $Q^2 > 1 \text{ GeV}^2$ , and on the  
 70 invariant mass of the hadronic final state  $W > 2 \text{ GeV}$ . The energy fraction of the incoming  
 71 lepton carried by the virtual photon  $y$  was limited to  $< 0.75$ . In addition, to reduce the  
 72 contribution from exclusive channels, the  $e'\pi^+X$  missing mass was required to be larger  
 73 than 1.5 GeV. For the multidimensional binning, first the electron variables are sorted in  
 74 9 bins in  $Q^2$  and  $x_B$  (see Fig. 2). For each of these  $Q^2 - x_B$  bins a binning is applied to  $z$   
 75 and  $P_T$  as shown for the example of  $Q^2 - x_B$  bin 1 in Fig. 2. The kinematic distributions  
 76 were found to be very similar for all 3 pions. Therefore the same binning scheme can be  
 applied to  $\pi^+$ ,  $\pi^-$  and  $\pi^0$ .

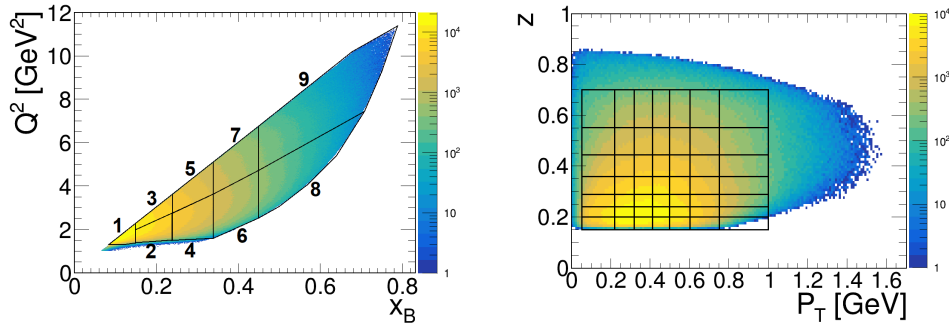


Figure 2: Left: Distribution of  $Q^2$  versus  $x_B$ . The bin boundaries are shown as black lines and the bin numbering is given. Right: Correlation between  $z$  and  $P_T$  for  $Q^2 - x_B$  - bin 1. The black lines indicate the bin borders. [10]

77

78 The beam SSA and its statistical uncertainty were determined experimentally from  
 79 the number of counts with positive and negative helicity ( $N_i^\pm$ ) in a specific bin  $i$  as:

$$SSA = \frac{1}{P_e} \frac{N_i^+ - N_i^-}{N_i^+ + N_i^-}, \quad \sigma_{SSA} = \frac{1}{P_e} \sqrt{\frac{1 - (P_e SSA)^2}{N_i^+ + N_i^-}}, \quad (4)$$

80

81 where  $P_e = 86.3\% \pm 2.6\%$  is the average magnitude of the beam polarization.  $A_{LU}^{\sin\phi}$  was  
 82 extracted by a fit of a  $\sin\phi$  function to the  $\phi$  dependence of the beam SSA. The obtained  
 83  $A_{LU}^{\sin\phi}$  moment is then related to  $F_{LU}^{\sin\phi}/F_{UU}$  via Eq. (2). Several sources of systematic un-  
 84 certainty were investigated, including beam polarization, radiative effects, particle iden-  
 85 tification and contamination from baryon resonances and exclusive  $\rho$  meson production.  
 86 A detailed Monte Carlo simulation was performed to study acceptance and bin-migration  
 87 effects, which were both found to be negligible compared to the other contributions. The  
 88 influence of additional azimuthal modulations  $\cos\phi$  and  $\cos 2\phi$  on the extracted  $\sin\phi$  am-  
 89 plitude was also evaluated, and found to be negligible. More details can be found in [10].

### 90 3 Results

91 The structure function ratio  $F_{LU}^{\sin\phi}/F_{UU}$  has been extracted for each of the obtained 344  
 92 bins. Figure 3 shows the  $z$  and  $P_T$  dependencies of  $\pi^+$  for selected  $P_T$  and  $z$  bins in  
 93 different bins of  $Q^2$  and  $x_B$  (bin 1:  $Q^2 = 1.71 \text{ GeV}^2$ ,  $x_B = 0.13$ , bin 2:  $Q^2 = 2.02 \text{ GeV}^2$ ,  
 $x_B = 0.19$ , bin 7:  $Q^2 = 4.89 \text{ GeV}^2$ ,  $x_B = 0.39$ , bin 9:  $Q^2 = 6.55 \text{ GeV}^2$ ,  $x_B = 0.52$ ).

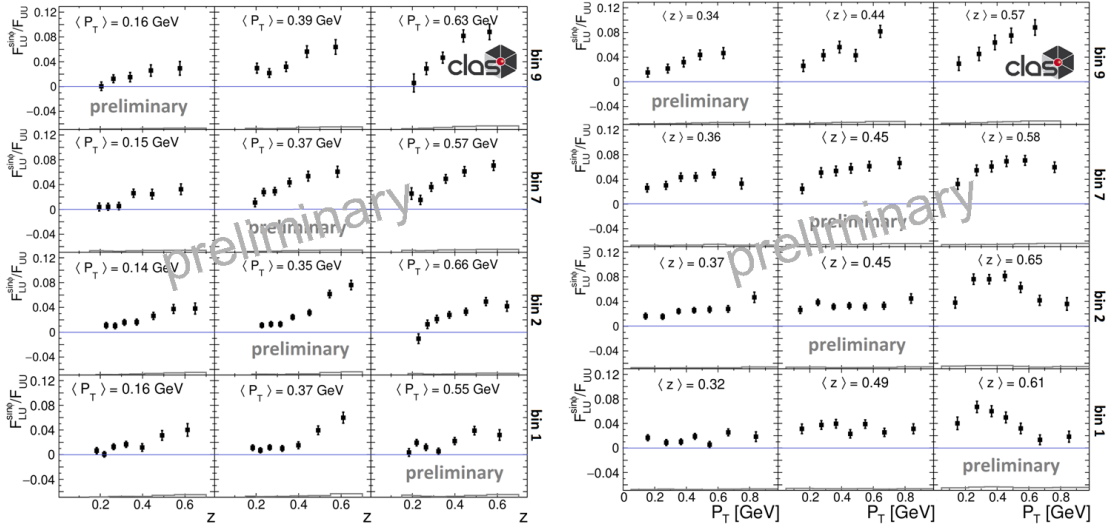


Figure 3:  $z$  dependence (left) and  $P_T$  dependence (right) of  $F_{LU}^{\sin\phi}/F_{UU}$  for  $\pi^+$  in increasing  $P_T / z$  bins (left to right) and for different  $Q^2$ - $x_B$  bins. The systematic uncertainty is given by the histogram above the horizontal axes.

94

95 For  $\pi^+$  it can be observed that the  $z$  dependence changes from a more flat behaviour  
 96 at small  $P_T$ ,  $Q^2$ , and  $x_B$  values to a steep increase at large  $P_T$ ,  $Q^2$ , and  $x_B$  values. Also  
 97 for the  $P_T$  dependence a small magnitude with a nearly flat behaviour can be observed  
 98 at small  $Q^2$ ,  $x_B$ , and  $z$  values, while for increasing  $z$  values a peaking structure with  
 99 varying mean value and width can be observed at small  $Q^2$  and  $x_B$ , while an increasing  
 100 trend becomes dominant at large  $Q^2$  and  $x_B$  values. Detailed comparisons to TMD based  
 101 theoretical models are available for the case of  $\pi^+$  in Ref. [10].

102

103 Preliminary results for the  $z$  and  $P_T$  dependence of  $\pi^0$  and  $\pi^-$  are shown in Fig. 4.  
 104 The same multidimensional bins as for  $\pi^+$  in Fig. 3 are used. For  $\pi^0$  a positive  $F_{LU}^{\sin\phi}/F_{UU}$   
 105 value can be observed, which has a similar magnitude as for  $\pi^+$ . However some differences  
 106 like a different trend and different structures of the  $P_T$  dependence in some bins can be  
 107 identified. In contrast to this,  $F_{LU}^{\sin\phi}/F_{UU}$  shows mostly negative values which are close  
 108 to zero for  $\pi^-$  at high  $Q^2$  and  $x_B$  values (bin 7 and 9). However at lower  $Q^2$  and  $x_B$   
 109 values (bin 1 and 2) sign transition occur between small and large  $P_T$  values as well as  
 110 between small and large  $z$  values. In the kinematic domain of large  $z$  and small  $P_T$  values,  
 111 a positive magnitude of up to 0.1 is reached, while at small  $z$  and intermediate to large  $P_T$   
 112 negative values with a typical order of -0.02 are observed. For  $\pi^0$  and  $\pi^-$  more detailed  
 studies of the systematic uncertainty are still ongoing.

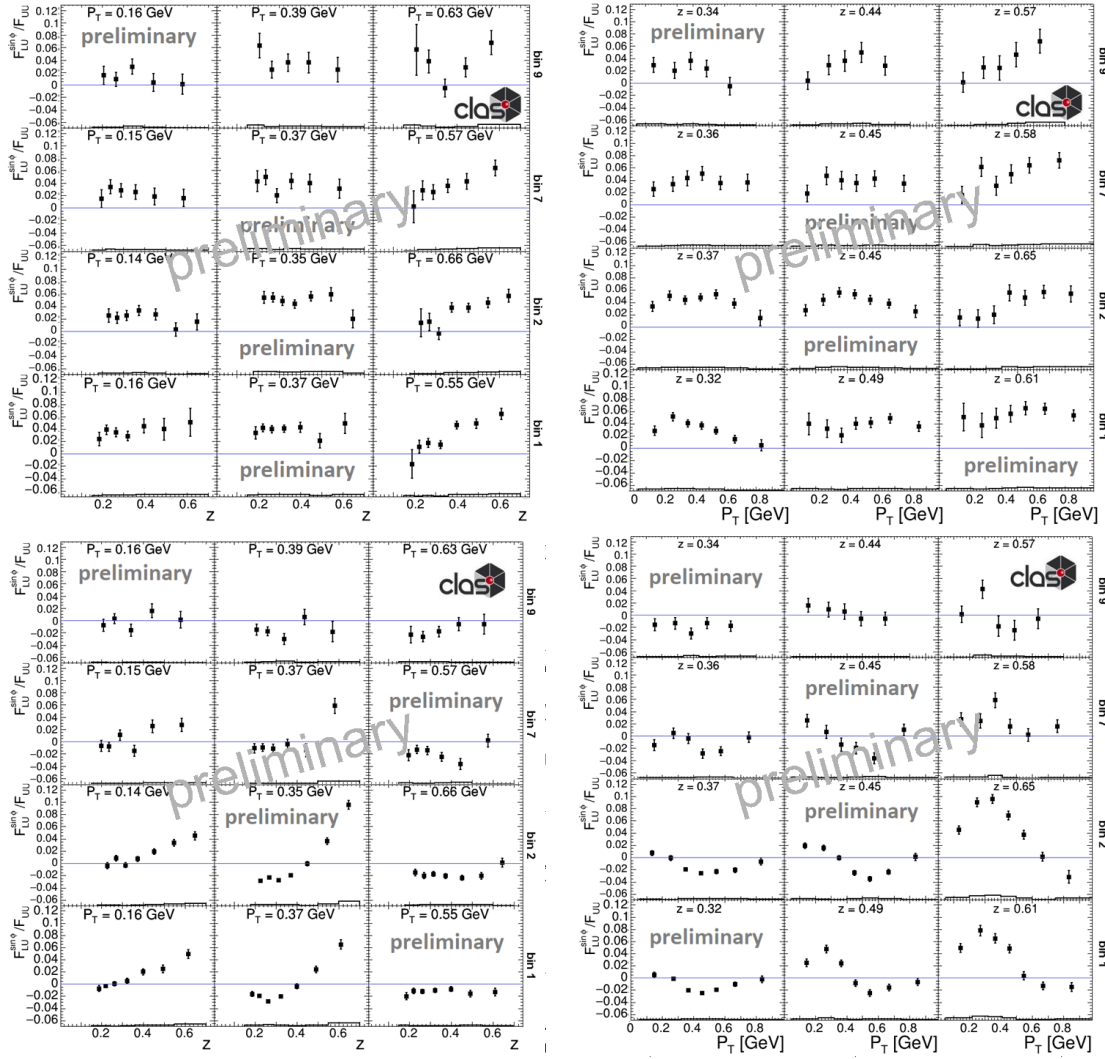


Figure 4: **Upper panels:**  $z$  dependence (left) and  $P_T$  dependence (right) of  $F_{LU}^{\sin \phi} / F_{UU}$  for  $\pi^0$  in different  $P_T / z$  and  $Q^2-x_B$  bins. **Lower panels:**  $z$  dependence (left) and  $P_T$  dependence (right) of  $F_{LU}^{\sin \phi} / F_{UU}$  for  $\pi^-$  in different  $P_T / z$  and  $Q^2-x_B$  bins. A preliminary estimate of the systematic uncertainty is given by the histogram above the horizontal axes.

## 113 4 Conclusion

114 In summary, the structure function ratio  $F_{LU}^{\sin \phi} / F_{UU}$  corresponding to the polarized elec-  
 115 tron beam single spin asymmetry in semi-inclusive deep inelastic scattering has been mea-  
 116 sured for all three pions over a wide range of kinematics in a fully multidimensional study.  
 117 The fully differential study revealed structures, which were not visible in previous inte-  
 118 grated studies like [11]. Including these multidimensional measurements into global fits,  
 119 in combination with future measurements of unpolarized cross sections, as well as polar-  
 120 ized target spin asymmetries, will provide new, strong constraints on the participating  
 121 TMDs and FFs. The high precision of the fully multidimensional measurement, enables a  
 122 detailed comparison to theoretical models for the first time. More details on this aspect  
 123 can be found in Ref. [10]. More detailed comparisons for all three pions in contrast to  
 124 theoretical models and the interpretation of the underlying physics effects will follow once  
 125 the studies of the systematic uncertainty of  $\pi^0$  and  $\pi^-$  are completed.

## 126 Acknowledgements

127 We acknowledge the outstanding efforts of the staff of the Accelerator and the Physics  
128 Divisions at Jefferson Lab in making this experiment possible.

129 **Funding information** This work was supported in part by the U.S. Department of En-  
130 ergy, the National Science Foundation (NSF), the Italian Istituto Nazionale di Fisica Nucle-  
131 are (INFN), the French Centre National de la Recherche Scientifique (CNRS), the French  
132 Commissariat pour l’Energie Atomique, the UK Science and Technology Facilities Council,  
133 the National Research Foundation (NRF) of Korea, the Helmholtz-Forschungsakademie  
134 Hessen für FAIR (HFHF) and the Ministry of Science and Higher Education of the Rus-  
135 sian Federation. The Southeastern Universities Research Association (SURA) operates  
136 the Thomas Jefferson National Accelerator Facility for the U.S. Department of Energy  
137 under Contract No. DE-AC05-06OR23177.

## 138 References

- 139 [1] J. Gao, L. Harland-Lang and J. Rojo, Phys. Rept. **742**, 1 (2018).  
140 [2] J. J. Ethier and E. R. Nocera, Annu. Rev. Nucl. Part. Sci. **70**, 43 (2020).  
141 [3] K. Goeke, A. Metz and M. Schlegel, Phys. Lett. B **618**, 90 (2005).  
142 [4] A. Bacchetta *et al.*, JHEP **02**, 093 (2007).  
143 [5] A. Metz *et al.*, Prog. Part. Nucl. Phys. **91**, 136 (2016).  
144 [6] B. Pasquini and S. Rodini, Phys. Lett. B **788**, 414 (2019).  
145 [7] J. Levelt and P. J. Mulders, Phys. Lett. B **338**, 357 (1994).  
146 [8] M. Anselmino, A. Mukherjee, and A. Vossen, Prog. Part. Nucl. Phys. **114**, 103806  
147 (2020).  
148 [9] V. D. Burkert *et al.* (CLAS Collaboration), NIM A **959**, 163419 (2020).  
149 [10] S. Diehl *et al.* (CLAS Collaboration), "First multidimensional, high precision mea-  
150 surements of semi-inclusive  $\pi^+$  beam single spin asymmetries from the proton over a  
151 wide range of kinematics", submitted to Phys. Rev. Lett. (2021). arXiv:2101.03544  
152 [11] W. Gohn *et al.* (CLAS Collaboration), Phys. Rev. D **89**, 072011 (2014).